PAPER

Shearless transport barriers in magnetically confined plasmas

Plasma Phys. Control. Fusion **54** (2012) 124035 (6pp) doi:10.1088/0741-3335/54/12/124035

Shearless transport barriers in magnetically confined plasmas

I L Caldas[1], R L Viana[2], C V Abud[1], J C D Fonseca[1], Z O Guimarães Filho[1,3], T Kroetz[4], F A Marcus[3], A B Schelin[5], J D Szezech Jr[6], D L Toufen[1,7], S Benkadda[3], S R Lopes[2], P J Morrison[8], M Roberto[9], K Gentle[8], Yu Kuznetsov[1] and I C Nascimento[1]

[1] Instituto de Física, Universidade de São Paulo, São Paulo, SP, Brazil
[2] Departamento de Física, Universidade Federal do Paraná, Curitiba, Paraná, Brazil
[3] IIFS-PIIM, CNRS-Aix Marseille Universite, Marseille, France
[4] Departamento de Física, Universidade Tecnológica Federal do Paraná, Pato Branco, PR, Brazil
[5] Departamento de Física, Universidade Tecnológica Federal do Paraná,Curitiba, PR, Brazil
[6] Departamento de Matemática e Estatística, Universidade Estadual de Ponta Grossa, Ponta Grossa, PR, Brazil
[7] Instituto Federal de Educação Científica e Tecnológica de São Paulo, Guarulhos, SP, Brazil
[8] Department of Physics, The University of Texas at Austin, TX, USA
[9] Instituto Tecnológico de Aeronáutica, São José dos Campos, SP, Brazil

E-mail: viana@fisica.ufpr.br

Received 20 June 2012, in final form 21 September 2012
Published 21 November 2012
Online at stacks.iop.org/PPCF/54/124035

Abstract
Shearless transport barriers appear in confined plasmas due to non-monotonic radial profiles and cause localized reduction of transport even after they have been broken. In this paper we summarize our recent theoretical and experimental research on shearless transport barriers in plasmas confined in toroidal devices. In particular, we discuss shearless barriers in Lagrangian magnetic field line transport caused by non-monotonic safety factor profiles. We also discuss evidence of particle transport barriers found in the TCABR Tokamak (University of São Paulo) and the Texas Helimak (University of Texas at Austin) in biased discharges with non-monotonic plasma flows.

(Some figures may appear in colour only in the online journal)

1. Introduction

Internal transport barriers cause a localized reduction of particle and energy transport in fluids and plasmas [1, 2]. Among the key factors responsible for the formation of internal transport barriers is the existence of a non-monotonic flow profile, which gives rise to reversed shear flows and the formation of shearless curves. These curves act as dikes preventing chaotic particle transport across them, and so are identified as shearless transport barriers. The essentials of a system exhibiting shearless transport barriers are exhibited by a simple two-dimensional mapping called standard nontwist map [3].

Shearless transport barriers also have been found in magnetically confined plasmas with reversed shear [4]. For example, non-monotonic radial profiles of the electric current in tokamaks lead to a reversal of the magnetic shear and thus a shearless curve [5]. In the presence of chaotic transport of particles and energy these shearless curves act as internal transport barriers. Even after these barriers have been broken the remaining islands may present a large stickness that decreases transport [6]. Magnetic field line Hamiltonian models of reversed shear plasmas present a violation of the twist condition and hence are also classified as nontwist systems [4]. Another example of shearless barriers in confined plasmas is a non-monotonic electric field profile causing a reversed shear flow described by the $\boldsymbol{E} \times \boldsymbol{B}$ radial drift motion of particles [7].

In this paper we review some of the aspects of shearless transport barriers in plasmas, focusing on the abovementioned examples. Section 2 begins with a more general discussion of transport barriers in the standard nontwist map, which is a paradigmatic model for sheared flows in fluids and plasmas. Section 3 presents results on the formation of

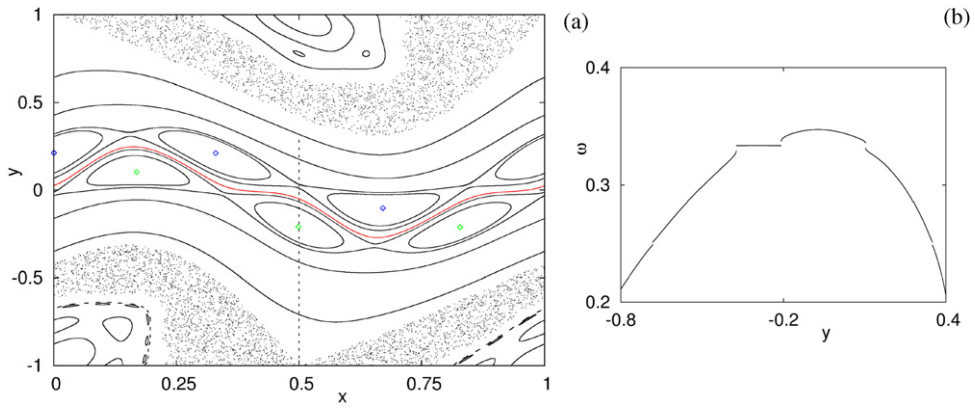

Figure 1. (*a*) Phase portraits for the SNTM with $a = 0.358$ and $b = 0.354$; (*b*) winding number profile corresponding to the dashed vertical line in (*a*).

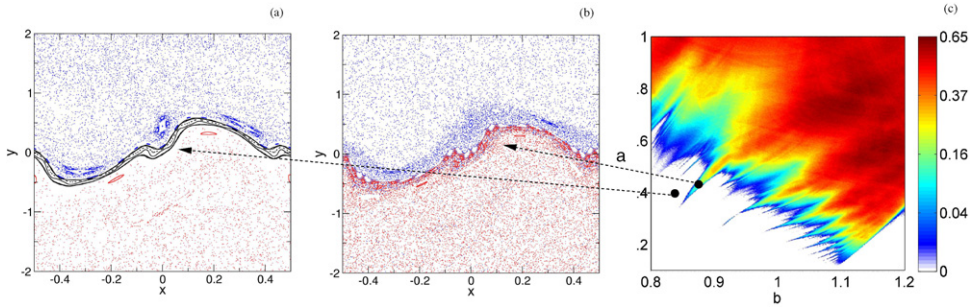

Figure 2. Phase portraits for the SNTM with (*a*) $a = 0.40$, $b = 0.85$ and (*b*) $a = 0.42$, $b = 0.88$. (*c*) Transmissivity of the shearless transport barrier as a function of the parameters of the SNTM.

shearless transport barriers in plasma models with non-monotonic profiles. Section 4 considers chaotic particle transport in a plasma model due to electrostatic drift waves and a non-monotonic electric field profile. Section 5 discusses experimental evidence of internal transport barriers in the TCABR. Section 6 presents evidence of transport barriers in the Texas Helimak after changing the radial electric field profile. The last section is devoted to our conclusions.

2. Transport barriers in nontwist maps

The fundamental concepts underlying the formation of shearless transport are displayed by the so-called standard nontwist map (SNTM) [3, 4, 8] $(x_{n+1}, y_{n+1}) = (x_n + a(1 - y_{n+1}^2), y_n - b\sin(2\pi x_n))$, where $0 \leqslant x \leqslant 1$, $a > 0$ and $b > 0$ are parameters. The variables (x_n, y_n) can be regarded as the normalized angle and action, respectively, of a phase space trajectory of a Hamiltonian system at its nth piercing with a Poincaré surface of section. It follows that the SNTM is area-preserving.

The function $g(y) = a(1 - y^2)$ appearing in the SNTM is the winding number of the unperturbed trajectories lying on nested tori, and $g'(y)$ stands for the shear. Since g presents a non-monotonic behavior the corresponding shear changes sign at those points $(x_s, y_s = 0)$ for which $g'(y_s) = 0$, defining the so-called shearless curve. The existence of such a shearless curve violates locally the twist condition, and hence not all features of twist systems (such as KAM theorem and Aubry–Mather theory) apply.

If $b \neq 0$ two main island chains show up on each side of a shearless invariant curve roughly around $y_s = 0$ (depicted in red in figure 1(*a*)). The exact location of this shearless curve depends on x and it turns out to be the local maximum of the perturbed winding number for a fixed x (figure 1(*b*)). In addition to these two main island chains there are other chains, with considerably large chaotic layers due to the homoclinic tangle therein. These chaotic layers are not connected, since there are invariant curves near the shearless invariant curves preventing global transport.

As the perturbation strength increases further (figure 2(*a*)) the island chains on each side of the shearless curve are practically destroyed, leaving two regions of chiefly chaotic motion therein, separated by a number of invariant curves surrounding the shearless curve. Even after these invariant curves are destroyed, for higher perturbation intensity, there is an effective transport barrier in the place of the former shearless curve due to the strong stickness effect (figure 2(*b*)) [6].

In order to quantify the transmissivity of the shearless transport barrier formed after the shearless curve has been destroyed we have computed the fraction of phase points crossing the former shearless curve. We randomly chose a large number of initial conditions on the line $(-0.5 < x_B < 0.5, y = 1.0)$ and iterated the resulting orbits for a long time $N = 50\,000$ (if the N value is chosen large enough to evidence the stickness effect of the broken barrier, the parameter space shown in figure 2(*c*) does not depend on N). Then we counted the number of orbits that crossed the broken shearless curve reaching the $y = -1$ line. The transmissivity as a function of a and b is depicted in figure 2(*c*). The two black dots represent

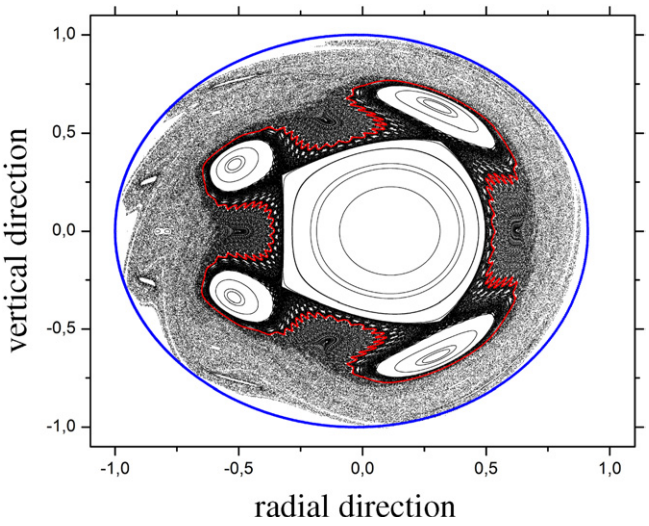

Figure 3. Phase portrait of the Poincaré map for a tokamak with a non-monotonic current profile and an ergodic magnetic limiter.

the phase portraits shown in figures 2(*a*) and (*b*). White pixels denote zero transmissivity, i.e. the shearless curve has not been destroyed yet, which is the case of figure 2(*a*). The boundary of the zero transmissivity region is highly complex and has been determined using renormalization techniques [3].

3. Transport barrier in nontwist magnetic field

As illustrated in the previous discussion of the SNTM, the key factor in the formation of an internal transport barrier is the appearance of a shearless curve due to some non-monotonic profile characterizing the system. This shearless curve, whenever it exists, is a perfect barrier. However, even though this curve may be broken, there remains a barrier effect due to the stickness of trajectories in its vicinity. In this section we shall describe some models for magnetic field lines in tokamaks with nontwist properties (non-monotonic profiles) that exhibit shearless transport barriers.

Magnetic field lines in toroidal systems such as tokamaks lie on constant pressure surfaces characterized by a poloidal flux function Ψ which satisfies the equilibrium Grad–Shafranov equation. Using non-orthogonal coordinates (r_t, θ_t) equilibrium flux surfaces depend on r_t only, at lowest order approximation. The intersections of flux surfaces with a toroidal plane $\varphi = \text{const}$ are non-concentric circles with a shift toward the exterior equatorial region [9]. We have considered an equilibrium solution for the Grad–Shafranov equation using a non-monotonic toroidal current density profile.

In terms of a Hamiltonian formulation of magnetic field lines, the coordinates (r_t, θ_t) are related to the action and angle variables, respectively, of the equilibrium configuration, the toroidal coordinate φ playing the role of time, and the flux function $\Psi(r_t)$ is, up to a constant factor, an integrable Hamiltonian [4, 11]. The addition of magnetic perturbing fields introduces non-integrable contributions to this Hamiltonian and, in this specific case, we have used fields created by an ergodic magnetic limiter [12]. The limiter current can be taken as the perturbation strength. The magnetic field line equations can be written as canonical equations from the Hamiltonian, and we can make a Poincaré plot by tracing the intersections of the field lines with a poloidal plane $\varphi = 0$ (see [10] for details of the equations and parameter values).

In figure 3 we plot the phase portrait of the resulting Hamiltonian system for parameters of the TCABR. Due to the non-monotonic safety factor radial profile there is, in the equilibrium configuration, a shearless torus (corresponding to a shearless curve, depicted in red in figure 3) at the local minimum of the safety factor profile. The ergodic limiter field excites modes on both sides of this shearless curve and, as the perturbation is strong enough, a large chaotic region exists in the outward side of the shearless curve (the ergodic limiter causes a stronger perturbation near the plasma edge). However, even with strong perturbation the shearless curve meanders along the torus and is an internal transport barrier [13, 14].

The previous model takes into account a number of details for both equilibrium and perturbing magnetic fields. The complexity of the resulting field line equations demands the use of numerical methods to obtain the Poincaré map [10]. However, it is possible to derive an analytical map for simpler models, yet preserving the essential physical features present in more sophisticated models [15]. One such example is the area-preserving Ullmann map, whose analytical expressions can be found in [16].

Just like the numerical map shown in figure 3, the perturbation caused by the limiter provokes the creation of a large chaotic region near the tokamak wall (figure 4(*a*)). Moreover, the non-monotonicity of the safety factor produces a shearless transport barrier, indicated as a green curve in figure 4(*a*) (see also a magnification in figure 4(*b*), showing the chaotic region above the barrier), that remains active even after the shearless curve has been destroyed after increasing further the perturbation strength.

In a lowest order approximation plasma particles follow the magnetic field lines with no collisions. The latter make the gyroradii of particles suffer randomly oriented displacements and so too corresponding guiding centers. Thus we can phenomenologically describe particle collisions in the Ullmann map by adding a random noise term (to both variables) after each map iteration [17, 18]. Figure 4(*c*) illustrates the addition of such noise term in the chaotic region above the barrier of figure 4(*b*) (computed without noise).

It is worth noting that the presence of shearless barrier is a consequence of extrema of winding number profiles. In non-monotonic plasma profiles there is a global minimum of safety factor profile related to a robust shearless barrier near the plasma edge, this global minimum being a global extremum of the winding number. However, even for twist maps local extrema may exist allowing a secondary formation of shearless barriers of limited extent. An example is provided by the Ullmann map, where the safety factor profile has been replaced by a monotonic function. A phase portrait of this twist map shows a large chaotic region near the plasma edge, as expected from an ergodic limiter (figure 5(*a*)). If we analyze the island remnants buried inside the chaotic region, shearless barriers of limited extent appear inside the islands (the green curve in figure 5(*b*)) as a result of local extrema of the corresponding winding number profile (figure 5(*c*)).

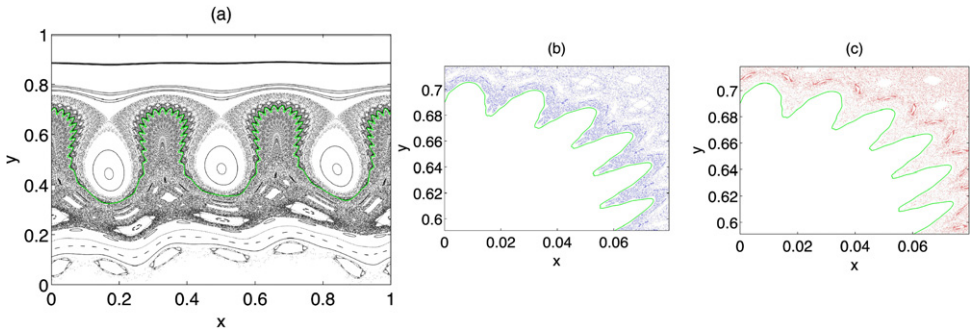

Figure 4. (*a*) Phase portrait of the Ullmann map; (*b*) magnification of a region of (*a*); (*c*) the same region with noise and the barrier of (*b*) copied here to guide the eye.

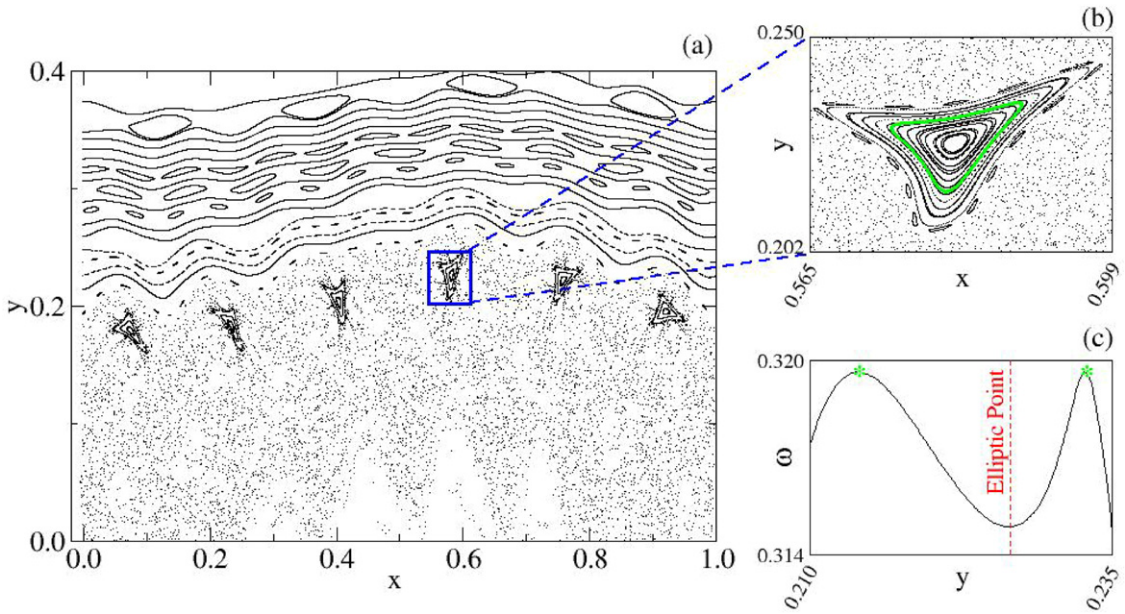

Figure 5. (*a*) Phase portrait of the Ullmann map; (*b*) magnification of a portion of (*a*); (*c*) local winding number profile of the island in (*b*), indicating local extrema.

4. Particle transport in plasmas

A substantial improvement in the plasma confinement has been observed in many Tokamaks when the radial electric field profile is modified by the introduction of a bias electrode [19]. In tokamaks with edge biasing polarization a strong decrease in the low-frequency component of the fluctuating floating potential and turbulent-driven particle flux [20] has been observed. These results motivate the use a drift Hamiltonian model to investigate particle transport reduction due to a shearless internal transport barrier caused by a non-monotonic electric field profile. Although the description of turbulent systems would require the use of many degrees of freedom, it turns out that some essential features of turbulent systems, such as the coexistence of many asymptotic states, can be described by low dimensional systems [21].

Let us consider, in the slab approximation (large aspect ratio tokamak near the plasma edge region), a uniform magnetic field along the toroidal (z) direction and the particle guiding center $\boldsymbol{E} \times \boldsymbol{B}$ drift in the poloidal (y) direction. Due to the radial (x) particle density gradient in the plasma edge, a perturbed electric field gives rise to electrostatic waves responsible for the radial particle drifts. We thus assume an electrostatic potential of the form $\phi(x, y, t) = \phi_0(x) + A \sin(k_x x) \cos(k_y y - \omega t)$, where ϕ_0 is a background equilibrium potential for the non-monotonic radial electric field and A, $\boldsymbol{k}$ and ω are, respectively, the amplitude, wave number and frequency of a drift wave propagating in the poloidal direction [22]. The particle equations of drift motion can be regarded as canonical equations from a Hamiltonian function and have been numerically solved [7, 23].

The intersections of particle trajectories with a Poincaré surface of section are depicted in figure 6(*a*). Since $\phi_0(x)$ has a non-monotonic profile the drift-wave Hamiltonian does not fulfill the twist condition for all points in the radial direction and thus a shearless curve appears as an internal transport barrier (the black curve in figure 6(*a*)). The regions with large radial transport can be described by the so-called trapping function $U(x)$, with a non-monotonic radial profile, with a maximum corresponding to a shearless barrier roughly around $x = 2$ (figure 6(*b*)) [7]. On both sides of the shearless barrier the profiles are monotonic and twin island chains are formed. The zeroes of the trapping function represent resonances, for which the phase velocity of one wave matches the $\boldsymbol{E} \times \boldsymbol{B}$ drift velocity.

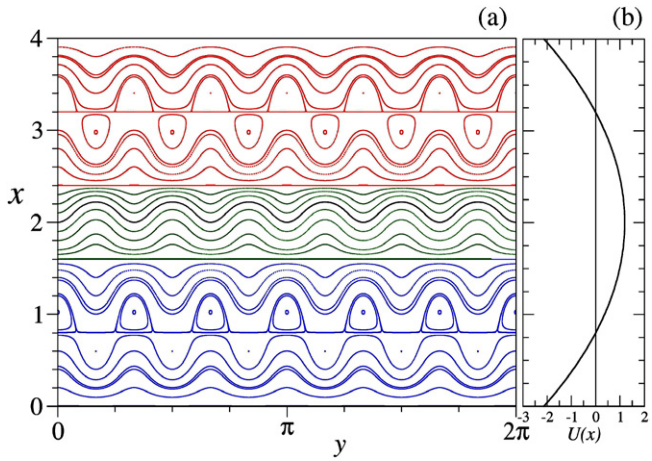

Figure 6. (*a*) Phase portrait for a one-wave drift Hamiltonian; (*b*) radial profile of the trapping function.

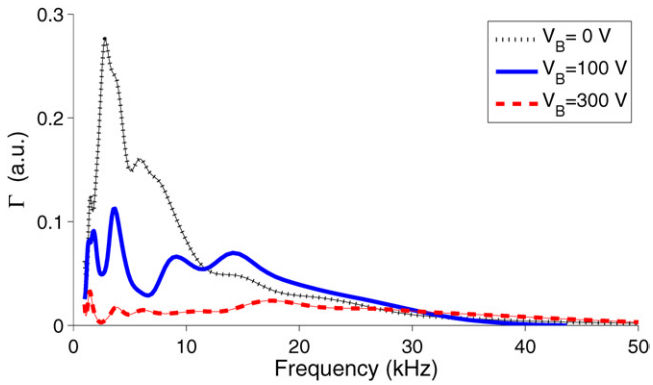

Figure 7. Spectral contribution of the turbulent-driven radial particle flux in TCABR tokamak with and without electrode biasing.

5. Particle transport in TCABR tokamak

If the shearless barrier is located in the scrape-off layer near the tokamak wall then the transport reduction is not so effective. However, if a bias electrode is activated it turns out that the electric field profile changes and the trapping profile is radially displaced, such that the shearless transport barrier can be placed at a desired position inside the plasma. Moreover, a biased electrode causes an enhancement of the maximum value of the trapping function, extending the region with transport barriers and, consequently, increasing the transport reduction. The improvement of the transport barrier after the use of a biased electrode has been observed in the TCABR through a decrease in the turbulent-induced particle flux measured in the scrape-off layer [7].

Figure 7 shows the spectral contribution of the turbulent-driven radial particle flux in the scrape-off layer of TCABR with different electrode bias voltages. Without biasing the particle flux is chiefly observed at low-frequencies of ∼5 kHz, with an exponential-type decay for high frequencies. This spectral content is decreased with bias voltages of 100 and 300 V. These results are compatible with the inward displacement of a shearless barrier toward the tokamak edge, as the introduction of a bias electrode displaces the trapping function such that its maximum can be located inside the plasma, where a shearless barrier prevents turbulence-driven radial transport.

6. Evidence of transport barrier in Texas Helimak

The Texas Helimak is a toroidal device where the magnetic field is a composition of a main toroidal field and a small vertical field, such that the magnetic field lines are helices winding around the vessel and the plasma has a MHD equilibrium independent from plasma current [24]. Moreover, the plasma has a vertical velocity v_z whose radial profile is non-monotonic, such that its maximum is related to a shearless transport barrier. The magnetic shear can be computed as $(1/v_z)(\mathrm{d}v_z/\mathrm{d}R)$, where R stands for the radial position measured from the Helimak vertical axis.

Biased electrodes have been used in Helimak to perturb the plasma equilibrium through a modification of the radial electric field profile. In figure 8(*a*) we plot two examples of radial profiles of the vertical velocity shear obtained for different values of the bias voltage. Such profiles were drawn from the velocity profile measured by a Doppler spectrometer [25]. In the two examples there is a non-monotonic radial profile, with the transport barrier being formed at the radius where the velocity shear vanishes. Complementarily, figure 8(*b*) shows the turbulence-driven radial particle fluxes, obtained from the two shear profiles shown in figure 8(*a*), computed as indicated in [26]. In the two examples of figure 8 it is remarkable that the largest reduction of particle fluxes occurs around the shearless radial positions, where a transport barrier is predicted by the model presented in section 4. As in the results from the TCABR presented in the previous section, the displacement of the barrier position observed in Helimak also depends on the bias value (but the strength of the barrier does not increase with the biasing). It is in fact a strong support for the claim that the sheer existence of shearless barriers comes from rather general properties of the Hamiltonian structure of nontwist systems.

Another distinctive feature observed in the Helimak is the existence of waves propagating along the vertical direction. When the phase velocity of these waves matches the vertical plasma velocity there are resonant effects similar to those observed when the trapping function vanishes in the drift motion in a tokamak [27, 28]. In fact, as the resonance condition is not fulfilled, with different phase and plasma velocities, like in the results presented in sections 5 and 6, transport barriers are created in the plasma. In addition, the shearless barrier appears because the nontwist condition happens in the plasma.

While in the Texas Helimak the main cause of the transport reduction is a shearless barrier, in TCABR other barriers, created by almost resonant waves, also contribute to the transport reduction in addition to the shearless barrier. Moreover, in TCABR, increasing the bias voltage makes the reduction stronger because the barriers are displaced inward, reaching a plasma region with higher density. Furthermore, the transport could also be reduced by high flow shear as it has been predicted for monotonic zonal flows [20]. However, this last possibility is disregarded here because the peculiar nontwist condition in the zonal flow turns this effect into a

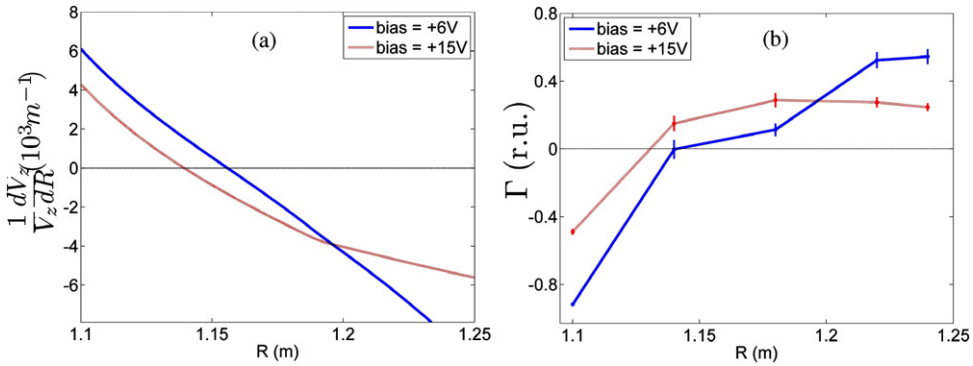

Figure 8. (*a*) Shear radial profile in Helimak discharges for two bias voltages. (*b*) Radial profile of turbulence-driven particle flux in Helimak for two bias voltages

secondary one. As in the results from the TCABR presented in the previous section, the displacement of the barrier position observed in Helimak also depends on the bias value (but the strength of the barrier does not increase with the biasing).

7. Conclusions

In this work we have summarized our recent theoretical and experimental work related to the formation of shearless transport barriers in toroidal plasmas. The underlying mechanism of such barriers is the non-monotonicity of radial profiles generating global and/or local maxima of the corresponding winding number profiles. In tokamaks, for example, non-monotonic plasma current profiles generate a shearless torus that, even after it has been broken, continues to act as an effective transport barrier due to the stickiness of trajectories. As we have shown in a twist map, even local maxima of winding numbers can be assigned to localized barriers inside magnetic islands, with a limited extent. These observations are also valid for drift motion of particle guiding centers due to electrostatic drift waves and a non-monotonic electric field profile.

The existence of shearless barriers has a direct impact on the transport in toroidal devices. In TCABR a biased electrode is able to create a non-monotonic electric field profile that reduces the radial particle flux driven by electrostatic turbulent fluctuations. Essentially the same observations were made in the Texas Helimak, where the non-monotonic profile of interest is related to the vertical velocity of the plasma. In both experiments the shearless regions are responsible for a decrease in the radial particle transport, hence improving the quality of confinement.

Acknowledgments

This work was made possible with help of the following Brazilian agencies: FAPESP, CNPq, CAPES, Fundação Araucária and CNEN-MCT (Brazilian Fusion Network). PJM was supported by US Department of Energy Contract # DE-FG05-80ET-53088.

References

[1] Sommeria J, Meyers S D and Swinney H L 1989 *Nature* **337** 58
[2] del-Castillo-Negrete D and Morrison P J 1993 *Phys. Fluids* A **5** 948
[3] del-Castillo-Negrete D, Greene J M and Morrison P J 1996 *Physica* D **91** 1
[4] Morrison P J 2000 *Phys. Plasmas* **7** 2279
[5] Oda G A and Caldas I L 1995 *Chaos Solitons Fractals* **5** 15
[6] Szezech Jr J D, Caldas I L, Lopes S R, Viana R L and Morrison P J 2009 *Chaos* **19** 043108
[7] Marcus F A, Caldas I L, Guimarães Filho Z O, Morrison P J, Horton W, Kuznetsov Y K and Nascimento I L 2008 *Phys. Plasmas* **15** 112304
[8] Fuchss K, Wurm A, Apte A and Morrison P J 2006 *Chaos* **16** 033120
[9] Kucinski M Y and Caldas I L 1987 *Z. Naturforsch.* A **42** 1124
[10] da Silva E C, Caldas I L and Viana R L 2001 *IEEE Trans. Plasma Sci.* **29** 617
[11] Balescu R 1998 *Phys. Rev.* E **58** 3781
[12] Caldas I L, Viana R L, Araujo M S T, Vannucci A, da Silva E C, Ullmann K and Heller M V A P 2002 *Braz. J. Phys.* **32** 980
[13] Kroetz T, Roberto M, da Silva E C, Caldas I L and Viana R L 2008 *Phys. Plasmas* **15** 092310
[14] Kroetz T, Marcus F A, Roberto M, Caldas I L and Viana R L 2009 *Comput. Phys. Commun.* **180** 642
[15] Viana R L and Caldas I L 1992 *Z. Naturforsch.* A **47** 941
[16] Portela J S E, Caldas I L, Viana R L and Morrison P J 2007 *Int J. Bifurcation Chaos* **17** 1589
[17] Rack M, Spatschek K H, Wingen A 2012 *Chaos* **22** 023114
[18] Schelin A, Caldas I L, Viana R L and Benkadda S 2011 *Phys. Lett.* A **376** 24
[19] Nascimento I C *et al* 2005 *Nucl. Fusion* **45** 796
[20] Van Oost G *et al* 2003 *Plasma Phys. Control Fusion* **45** 621
[21] Poon L and Grebogi C 1995 *Phys. Rev. Lett.* **75** 4023
[22] Horton W 1985 *Plasma Phys. Control Fusion* **27** 937
[23] del-Castillo-Negrete D 2000 *Phys. Plasmas* **7** 1702
[24] Gentle K W and Huang H 2008 *Plasma Sci. Technol.* **10** 284
[25] Rowan W L, Bespamyatnov I O and Granetz R S 2008 *Rev. Sci. Intrum.* **79** 10F529
[26] Ritz Ch P *et al* 1998 *Rev. Sci. Intrum.* **59** 1739
[27] Perez J C, Horton W, Gentle K W, Rowan W L, Lee K and Dahlburg R V 2006 *Phys. Plasmas* **13** 032101
[28] Toufen D, Guimarães Filho Z, Caldas I L, Marcus F A and Gentle K W 2012 *Phys. Plasmas* **19** 012307